TRENDS IN SCIENCES 2025; 22(8): 10106
https://doi.org/10.48048/tis.2025.10106 RESEARCH ARTICLE

A Circular Economy Use of Durian Rind Waste for Cellulose Extraction and Its Application in Polylactic Acid (PLA) Biodegradable Composites

Nawadon Petchwattana[1], Kamonchai Cha-aim[2], Khanet Rodphool[3], Puttaraksa Sang-on[2], Tuangphon Lapsarn[2], Jakkid Sanetuntikul[4] and Supaporn Sophonputtanaphoca[2,*]

[1]Department of Chemical Engineering, Faculty of Engineering, Srinakharinwirot University, Ongkharak Campus, Nakhon Nayok 26120, Thailand
[2]Division of Biotechnology and Agricultural Products, Faculty of Agricultural Product Innovation and Technology, Srinakharinwirot University, Ongkharak Campus, Nakhon Nayok 26120, Thailand
[3]Faculty of Agricultural Product Innovation and Technology, Srinakharinwirot University, Ongkharak Campus, Nakhon Nayok 26120, Thailand
[4]Faculty of Engineering and Technology, King Mongkut's University of Technology North Bangkok, Rayong Campus, Rayong 21120, Thailand

([*]Corresponding author's e-mail: supapornsp@g.swu.ac.th)

Received: 6 March 2025, Revised: 12 April 2025, Accepted: 19 April 2025, Published: 25 June 2025

Abstract

Durian rind is a food waste by-product left after consuming fruit flesh and can contribute to environmental pollution due to its slow decomposition and the large disposal area required because of its bulky shape. This study aims to evaluate the potential of durian rind as a cellulose source for producing biodegradable composites. Cellulose was extracted from the sample using a single-step alkali and hydrogen peroxide pretreatment under different conditions (temperature, residence time, and H_2O_2 concentration). The optimal condition for achieving the highest cellulose content with minimal lignin contamination was treatment with 5 % NaOH in 7.5 % H_2O_2 at 50 °C for 5 h. The extracted cellulose was milled and sieved to obtain 3 different particle sizes (< 250 µm (S), 250 - 425 µm (M), and > 425 µm (L)). All cellulose samples were characterized to determine their chemical and physical properties. FTIR spectra confirmed that most impurities in the raw material were removed after extraction. To evaluate the composite properties, polylactic acid (PLA)/cellulose composites with varying cellulose particle sizes and loadings were analyzed and compared to neat PLA. An increase in Young's modulus was observed with the addition of cellulose, with the effect being more pronounced at lower cellulose loadings. Conversely, higher cellulose content negatively affected the composite properties, reducing tensile strength and elongation at break. This adverse effect was more significant with larger cellulose particles. FE-SEM analysis revealed that larger cellulose particles created larger interfacial voids, contributing to a decrease in tensile elongation at break. The incorporation of cellulose into PLA slightly elevated the glass transition temperature by approximately 1 - 2 °C. Moreover, the degree of crystallinity (X_c) significantly increased with the addition of cellulose, with smaller cellulose particles being more effective in enhancing X_c. PLA/cellulose composites may be suitable for applications as single-use plastics.

Keywords: Circular economy, Waste, Biodegradable polymer, Environmental sustainability, Cellulose, Durian rind

Introduction

Biodegradable composites typically consist of lignocellulose-derived fibers and biopolymers, such as polylactic acid (PLA). PLA is synthesized through the polymerization of D-lactic acid and L-lactic acid enantiomers and can be produced via both fermentation and chemical processes [1,2]. As a natural polyester, PLA is biodegradable and possesses several desirable characteristics, including non-toxicity, biocompatibility,

mechanical strength, thermal stability, and environmental friendliness, making it particularly suitable for food packaging applications [3]. PLA exhibits physical properties such as stiffness, tensile strength, and gas permeability that are comparable to those of conventional plastics like polypropylene (PP) and polyethylene terephthalate (PET) [4]. However, its application in food packaging is limited by relatively low impact strength and elongation at break. To overcome these limitations, reinforcing PLA with cellulose has been shown to enhance its mechanical performance and extend its functionality in food packaging systems [5].

Additives such as cellulose or starch in PLA composites have been shown not to affect the diversity or total biomass of soil-dwelling bacteria and fungi when measured by soil weight [2]. Reinforcing PLA with cellulose offers several advantages, including increased mechanical strength and reduced brittleness of the resulting composite materials. Cellulose fibers derived from both woody and non-woody plants such as kenaf, hemp, and pineapple leaves have been widely used in composite fabrication [6]. Numerous studies have explored the reinforcing potential of cellulose from various sources in PLA composites, including bacterial cellulose [7], microcrystalline cellulose [8], nanocrystalline cellulose [9], wood fiber [10], kenaf [11], bamboo, and sawdust [5]. Among these sources, agricultural residues represent a particularly promising option due to their abundance, low cost, and high cellulose content. Incorporating agro-waste such as fruit peels, vegetable waste, and grain husks into biopolymer matrices to produce value-added biomaterials, including bioplastics, contributes to the sustainable reduction of agro-waste and supports the principles of a circular economy [2]. However, fruit waste continues to pose a significant challenge for agro-waste management, depending on both the types and quantities of waste generated.

Durian (*Durio zibethinus*) is a seasonal fruit cultivated in tropical regions such as Thailand, Indonesia, Malaysia, and the Philippines [12]. While the edible part of the durian is its yellowish fruit flesh, the peel (rind) and seeds are typically discarded as waste [13]. The durian rind, including the spiky peel, forms the bulky outer layer of the fruit and constitutes a major portion of this waste [14]. Substantial quantities of durian peel are collected annually in these countries. In 2020, approximately 22,000 metric tons of durian fruit were produced, with the rind accounting for around 60 % of the fruit's total weight. This corresponds to an estimated 13,200 metric tons of durian rind waste in that year [15]. Due to its chemical composition, durian rind is classified as a lignocellulosic material with strong potential for conversion into high-value products. It has been reported to contain approximately 60.45 % cellulose, 15.45 % lignin, 13.09 % hemicellulose [15], and 4.20 % ash [16]. Given its high fiber content, durian rind represents a promising and underutilized source of natural cellulose, aligning with the principles of the circular economy and sustainable waste valorization.

Several studies have investigated the incorporation of durian rind fiber into polymer materials. For example, Penjumras *et al.* [17] examined the effect of cellulose derived from durian rind on the properties of PLA/cellulose composites. In their study, high cellulose loadings (25 - 35 wt%) with particle sizes ranging from 125 to 250 μm were applied. The results indicated that increasing cellulose content led to a higher Young's modulus and enhanced composite strength. Similarly, Halász and Csóka [9] characterized PLA/cellulose composites using microcrystalline cellulose with particle sizes smaller than 20 μm, both with and without ultrasound treatment, as well as cellulose nanoparticles. Their findings showed that smaller cellulose particles, due to their higher surface area, provided better interfacial adhesion, resulting in improved physical properties of the composites. Manshor *et al*. [13] investigated the effects of alkali pretreatment (4 % NaOH at room temperature for 1 h) on durian skin fiber and its influence on the mechanical and thermal properties of PLA/durian skin fiber composites. Their results showed that alkali-treated fibers significantly enhanced both the impact strength and thermal stability of the composites compared to those reinforced with untreated fibers. In addition to PLA, durian peel fiber has also been utilized to reinforce other biopolymer composites. Jumaidin *et al*. [14] examined the effects of varying durian peel fiber loadings (10 - 50 wt%) on the properties of cassava starch composites. Their findings revealed that increasing the fiber content improved thermal stability as well as tensile and flexural properties. The significance of fiber content in determining composite

properties was supported by Lee *et al.* [15], who evaluated the incorporation of different amounts of durian husk fiber into PLA composites.

Recently, durian rind has gained recognition as a local and natural source of cellulose for the production of biodegradable packaging materials. However, efficient methods for converting durian rind into such materials and for extracting high-purity cellulose from this agricultural waste are still lacking [12]. In the present study, durian rind (Monthong cultivar) was used as the raw material for cellulose production using a simple yet effective single-step pretreatment process at low temperatures. The optimal conditions of cellulose isolation were identified, and the extracted cellulose was characterized in terms of different particle sizes.

To the best of our knowledge, no prior research has specially addressed the impact of cellulose particle sizes greater than 250 μm on PLA/cellulose composites. These particle sizes were selected because their effect on composite performance has not yet been reported. Previous studies have shown that smaller cellulose particles improve composite properties due to increased surface area and better interfacial bonding [9,17]. In this work, we sought to determine whether such particle size-dependent effects remain valid at larger particle sizes, and to identify the practical limit of particle size for PLA composite reinforcement. Moreover, the use of larger cellulose particles offers potential benefits, including reduced energy consumption for size reduction and a simplified sample preparation process. This study aims to evaluate the influence of durian rind cellulose with particle sizes ranging from less than 250 μm to greater than 425 μm, at various loading levels, on the physical properties of PLA composites. The potential application of these composites in agricultural and food packaging was assessed based on their mechanical and thermal properties, as well as surface morphology.

Materials and methods

Raw material

Durian rind (*Durio zibethinus* Murray 'Monthong') was collected from a local market in Nakhon Nayok province, Thailand. The raw material was first cut into small pieces and sun-dried prior to being dried in a hot-air oven at 45 °C for 24 h. Dried biomass was milled by passing through a cutting mill (Retsch, Haan, Germany). It was then sieved through a 20-mesh sieve (particle size = 850 μm) and stored in a glass jar with a screw-capped lid at room temperature for use in all experiments.

Chemicals

All chemicals were laboratory reagent grade purchased from Sigma-Aldrich (Sigma Chemical Co., USA), UNIVAR (Ajax Finechem, Australia), chem-supply (ChemSupply Australia, South Australia), LABCHEM (Ajax Finechem, Australia), Loba Chemie (LOBA CHEMIE PVT. LTD., India), EMPLURA and EMSURE (Merck Millipore, Germany).

Determination of chemical composition of untreated durian rind

All chemical composition of durian rind was determined according to the Laboratory Analytical Procedures (LAP) issued by the National Renewable Energy Laboratory (NREL). Total solids, ash content, and extractives in the biomass were analyzed following the standard protocols [18-20]. Briefly, the biomass was subjected to exhaustive water and ethanol extraction (24 h for each process). After that, structural carbohydrate (cellulose) and lignin determination of the extractives-free sample was performed by a 2-step acid hydrolysis [21]. Cellulose content was quantified by measuring the amounts of glucose in the neutralized hydrolyzate using a glucose oxidase/peroxidase method (GOPOD assay kit, Megazyme, Ireland). Acid-soluble lignin (ASL) was investigated by the absorbance measurement at 320 nm and acid-insoluble lignin (AIL) was determined using the gravimetric method. All experiments were carried out in triplicate.

Isolation of cellulose

The method for cellulose isolation was slightly modified from Sophonputtanaphoca *et al*. [22]. To determine the optimal extraction conditions, approximately 0.3 g of dry durian rind sample was weighed and placed in a 20-mL scintillation vial. Ten mL of a pre-determined concentration of NaOH and H_2O_2 mixture was added to the vial, which was then sealed with a screw cap and placed in a rotating incubator at various residence times and temperatures (**Table 1**). To collect the solid phase for further experiments, the suspension was filtered through a

Gooch filter crucible (pore size = 10 - 12 µm). The solid residue was washed with distilled water, followed by 10 mL of 0.01 mM HCl and more distilled water to achieve a neutral pH before being dried in a hot-air oven at 45 °C for 24 h. The dried solid was used as a cellulose sample. Total solid recovery and total solid removal were measured in comparison to the dry weight of the biomass before extraction. The amounts of cellulose obtained from the different conditions were quantified as described below. The condition yielding the highest cellulose content was chosen as the optimal extraction condition for further study. All experiments were performed in triplicate.

Table 1 Conditions for cellulose isolation of durian rind.

Temperature (°C)	Time (h)	Concentration (%, w/v)
35	5	5 % NaOH in 2.5 % H_2O_2
	24	5 % NaOH in 5 % H_2O_2
		5 % NaOH in 7.5 % H_2O_2
		5 % NaOH in 10 % H_2O_2
50	5	5 % NaOH in 2.5 % H_2O_2
	24	5 % NaOH in 5 % H_2O_2
		5 % NaOH in 7.5 % H_2O_2
		5 % NaOH in 10 % H_2O_2
60	5	5 % NaOH in 2.5 % H_2O_2
	24	5 % NaOH in 5 % H_2O_2
		5 % NaOH in 7.5 % H_2O_2
		5 % NaOH in 10 % H_2O_2

Glucose analysis for quantification of cellulose content

The glucose analysis using the glucose oxidase/peroxidase (GOPOD) assay was modified from Sophonputtanaphoca *et al*. [22]. This assay was used to measure the cellulose content in both native biomass and extracted cellulose samples. Shortly, 50 µL of filtrate (neutralized hydrolysate obtained from the 2-step acid hydrolysis) was transferred into a test tube, and then 1000 µL of GOPOD reagent (GOPOD assay kit, Megazyme, Ireland) was added. Glucose solutions ranging from 0.2 to 0.8 mg/mL were used as standards. A reagent blank prepared with distilled water instead of the sample, served as a control. To develop the color resulting from the enzymatic reaction, the mixture was placed in an incubator at 40 °C for 20 min. Measurement of the absorbance was performed using a spectrophotometer with the wavelength of 510 nm. Cellulose content was calculated by multiplying the glucose amounts by a correction factor of 0.9, which accounts for the conversion from the monomeric to the polymeric form. The experiment was conducted in triplicate.

Preparation of different particle sizes of cellulose

Cellulose isolated under the optimal condition was used to reduce particle sizes. Various particle sizes of cellulose, including < 250 µm, 250 - 425 µm, and > 425 µm were prepared by milling the extracted cellulose with a milling machine (Retsch, Model: ZM 200, Haan, Germany). The milled cellulose was passed through a series of sieves with different mesh sizes: 40 mesh (on the top), 60 mesh (in the middle), and a receiving pan (on the bottom), all mounted on a sieving machine (Fritsch, Idar-Oberstein, Germany). Particles retained on the 40-mesh were used as the > 425 µm sample, while particles retained on the 60 mesh were used as the 250 - 425 µm sample. Particles that passed through the 60-mesh sieve and collected in the receiving pan were used as the < 250 µm sample.

Characterization of cellulose

Fourier-transform infrared (FTIR) analysis of cellulose was conducted to identify the functional groups in both the native durian rind sample and the extracted cellulose of different particle sizes. The

analysis was performed using FTIR spectrometer (Thermo Scientific, Model: Nicolet iS5, USA) in transmission mode, over wavelength range of 4000 - 400 cm^{-1}. The FTIR spectra of the cellulose samples were compared to those of the native durian rind.

X-ray diffraction (XRD) analysis was carried out to assess the crystallinity of the cellulose samples, following the procedures outlined by Rachtanapun *et al*. [23] and Haleem *et al*. [24]. Prior to testing, all samples were dried in a hot-air oven at 105 °C for 3 h. The analysis was performed over a scattering angle (2θ) range of 1 to 80 °, with a scanning rate of 5 °/min. The crystallinity of the cellulose was using the following equation:

$$\text{Crystallinity (\%)} = \frac{Crystallinity\ area \times 100}{Total\ area} \quad (1)$$

Scanning electron microscope (SEM) analysis was performed to examine the morphological structure of the cellulose surface using a scanning electron microscope (JEOL, JSM-IT300). All samples were gold-coated with gold and imaged at magnifications of 100×, 1000×, and 5000×.

Table 2 Blend formulation of PLA and cellulose.

Formulation	Cellulose content (wt%)		
	<250 µm (S)	**250 - 425 µm (M)**	**>425 µm (L)**
Neat PLA	-	-	-
S2.5	2.5	-	-
S5.0	5.0	-	-
S7.5	7.5	-	-
S10	10	-	-
M2.5	-	2.5	-
M5.0	-	5.0	-
M7.5	-	7.5	-
M10	-	10	-
L2.5	-	-	2.5
L5.0	-	-	5.0
L7.5	-	-	7.5
L10	-	-	10

Production and characterization of PLA/cellulose composites

An extrusion-grade PLA (Ingeo™ Biopolymer 2003D, NatureWorks LLC) was employed as the polymer matrix, with a melting temperature of 190 °C and a density of 1.32 g/cm^3. Cellulose in 3 particle size categories: Less than 250 µm (S), 250 - 425 µm (M), and greater than 425 µm (L) was used as additives. Each size fraction of cellulose particles was subsequently mixed with biodegradable PLA in concentrations ranging from 2.5 to 10 wt%.

As detailed in **Table 2**, each raw material was initially dry blended. The resulting blend compositions were then melt-mixed using a twin-screw extruder (Charoen Tut, E101) operating at a screw speed of 50 rpm. The temperature settings along the barrel, from zone 1 to zone 5, were maintained at 180, 190, 190, 210, and 210 °C, respectively. Following the melt mixing, the formulations were injected using an injection molding machine (Charoen Tut, INJ101T) for subsequent testing and characterization.

The visual appearance of PLA and its composites was captured using a Panasonic Lumix GF9 digital camera. The color fading of the composites in darkness was measured using a color meter (BYK Gardness, Color Flex) in terms of the L* value. The L* value

ranges from 0 to 100, where 0 indicates black and 100 indicates white.

Tensile testing was performed in accordance with ASTM D638 using a Universal Testing Machine (INSTRON, 5567) at room temperature. The test was conducted with a crosshead speed of 5 mm/min and a gauge length of 1 inch. The reported values represent the averages of ten replicated specimens. Additionally, the composites were analyzed using field-emission scanning electron microscopy (FE-SEM) (Hitachi, 4700e) to reveal the morphological structure of the composite surface.

The thermal and crystallization behaviors of neat PLA and PLA modified with cellulose were analyzed using a differential scanning calorimeter (DSC) (Perkin Elmer, DSC6000). The DSC measurements were conducted non-isothermally under the air atmosphere. Initially, the PLA and PLA/cellulose samples were heated from 25 to 210 °C to eliminate any thermal history. They were then held isothermally held at this temperature for 5 min. Subsequently, the samples were cooled down to 5 °C at a ramp rate of 5 °C/min and held at this temperature for 5 min before reheating to 210 °C. Data on the glass transition temperature (T_g), cold crystallization temperature (T_{cc}), and melting temperature (T_m) were recorded. The degree of crystallinity (X_c) was further calculated using Eq. (2) [25,26].

$$X_C(\%) = 100\frac{(\Delta H_m - \Delta H_c)}{\Delta H_f \times X_{PLA}} \quad (2)$$

where ΔH_m is the enthalpy of melting obtained from the area under the melting peak. ΔH_c is the enthalpy of crystallization obtained from the area under crystallization peak, and X_{PLA} is the weight fraction of PLA. ΔH_f is the heat of fusion, defined as the melting enthalpy of 100 % crystalline PLA, which was previously reported to be 93 J/g [25-27].

Statistical analysis

Averages and standard deviations (SD) were calculated using Microsoft Excel (Redmond, WA, USA). Statistical analysis was performed with SPSS software (ICN:793700) (version 22; IBM, Chicago, IL, USA), utilizing a one-way ANOVA and Duncan's Multiple Range Test (DMRT) at a 95 % confidence level.

Results and discussion

Chemical composition of native biomass

Table 3 presents the chemical composition of the durian rind sample used in this study. A high cellulose content, approximately 50 wt%, was found in the sample. The cellulose and other chemical components in native durian rind can vary depending on cultivars. For instance, Masrol *et al*. [28] reported that dried durian peel from Malaysia contained 31.6 % α-cellulose, 10.9 % lignin, and 5.5 % ash. Hasem *et al.* [29] revealed that the durian rind sample derived from the D118 (Durian Tembaga) cultivar contained 73.45 % cellulose. Charoenvai [16] reported that durian peel powder from Thailand was composed of 47.2 % holocellulose, 9.89 % lignin, 9.63 % hemicellulose, 4.20 % ash, 37.6 % hot-water solubility, and 18.9 % alcohol-benzene solubility. The chemical composition of the durian rind analyzed in this study was generally consistent with previous reports, with the exception of lignin content. Lignin is a complex phenolic polymer that contributes to the structural rigidity of plant cell walls. Through 2-step acid hydrolysis, structural carbohydrates and lignin are fractionated into forms that can be quantified more effectively. Lignin is separated into 2 components: An acid-soluble fraction (acid-soluble lignin) and an acid-insoluble fraction (acid-insoluble lignin) [21].

Table 3 Chemical composition of native durian rind. Data represent average ± standard deviation.

Component	% by dry weight of original biomass
Cellulose	49.9 ± 6.15
Acid-soluble lignin	2.01 ± 0.79
Acid-insoluble lignin	27.2 ± 3.92
Water extractives	22.5 ± 5.89
Ethanol extractives	12.9 ± 3.76
Ash	4.01 ± 1.03

Cellulose and lignin content after extraction

The durian rind sample was treated with sodium hydroxide (NaOH) at different concentrations of hydrogen peroxide (H_2O_2) and varied residence times and temperatures. The total solid recovery of all treatments is shown in **Figure 1**. Longer extraction times at elevated temperatures and higher concentrations of H_2O_2 resulted in higher total solid removal. At a 5-hour extraction, there was no significant difference in total solid recovery when the durian rind samples were treated with 5 % NaOH in either 2.5 % or 5 % H_2O_2 at 35 and 50 °C. However, higher concentrations of H_2O_2 (7.5 and 10 %) at a higher temperature (60 °C) caused more total solid removal. These effects were more pronounced when the durian rind samples were treated with all concentrations of H_2O_2 for a longer residence time (24 h), especially at the higher temperature (60 °C). The results of total solid removal were consistent with those of lignin removal (**Figure 2**).

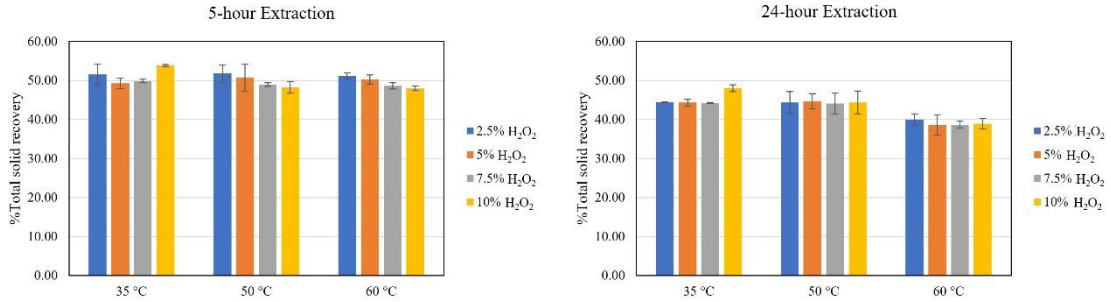

Figure 1 Comparison of total solid recovery in durian rind samples after extraction with 5 % NaOH in different concentrations of H_2O_2 at elevated temperatures for 5 and 24 h.

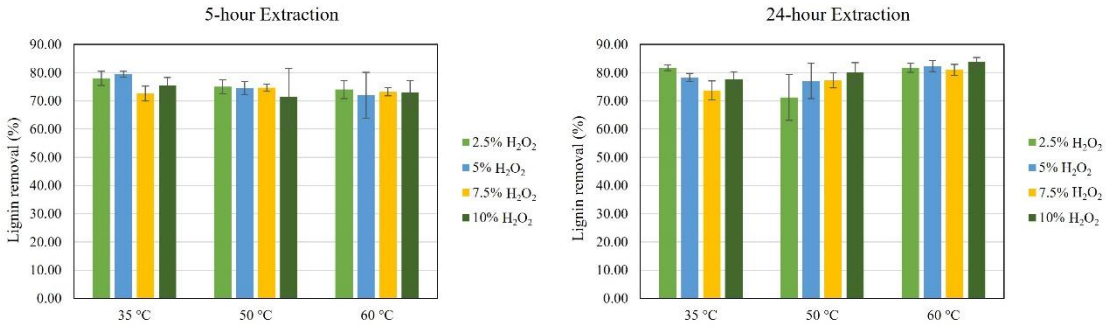

Figure 2 Comparison of lignin removal from durian rind samples after extraction with 5 % NaOH in different concentrations of H_2O_2 at elevated temperatures for 5 and 24 h.

Sophonputtanaphoca *et al.* [30] investigated the effect of alkali pretreatment on rice straw using 5 % NaOH at different residence times (1 - 5 h) and elevated temperatures (50 - 100 °C). The study revealed that elevated temperatures had a more significant impact than residence times, with higher temperatures resulting in greater total solid and lignin removal. This phenomenon is consistent with the findings of the present study. Alkali reagents play a crucial role in the delignification of lignocellulosic materials [31]. When combined with an alkali reagent, H_2O_2 in an aqueous solution solubilizes to form hydroxyl radicals (HO•), which react with lignin. This reaction causes delignification and generates low molecular weight, water-soluble lignin products [32]. Suriyatem *et al.* [33] further examined the effects of H_2O_2 delignification on palm bunch and bagasse using 0 - 40 % (v/v) H_2O_2 at 80 °C for 2 h. They found that perhydroxyl anion (HO_2^-) can contribute to a bleaching effect by generating perhydroxyl radicals (HO_2•), which may subsequently dissociate to form superoxide radical anions (O_2^-•)—highly reactive species capable of further degrading lignin. A schematic illustration of the delignification mechanism is presented in **Figure 3**.

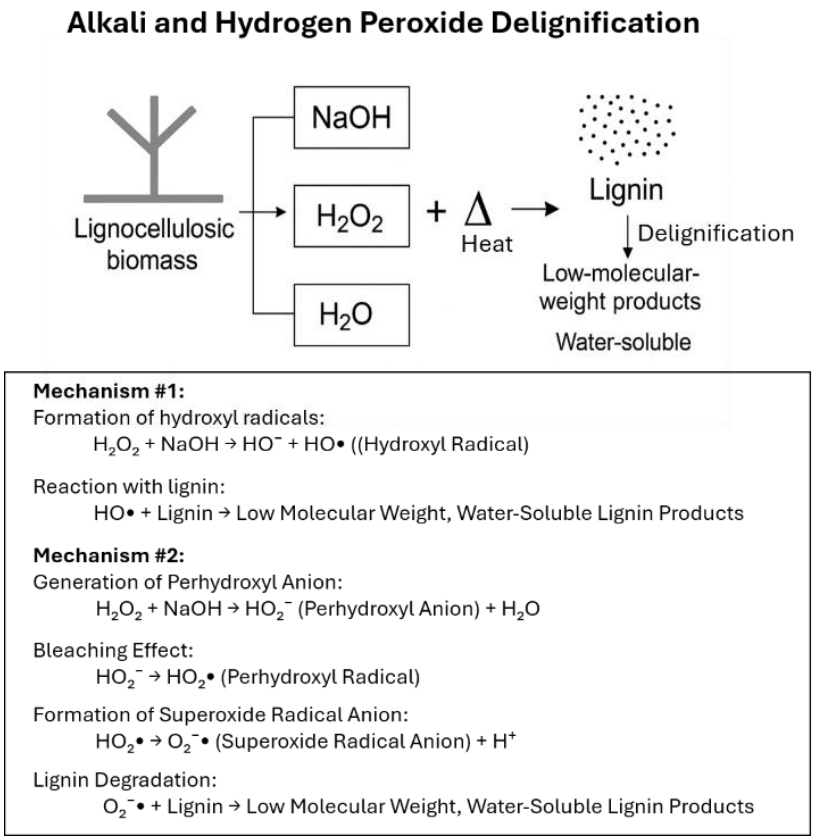

Figure 3 Schematic diagram illustrating the delignification mechanism during a single-step alkali and hydrogen peroxide pretreatment of lignocellulosic biomass.

It is worth noting that H_2O_2 is a highly unstable molecule that decomposes through a sequence of reactions. Its stability is influenced by various factors, including temperature, pH, exposure to light, and interactions with transition metals. H_2O_2 is more stable under acidic conditions, and increasing its concentration typically lowers the pH of the solution [34]. The decomposition of H_2O_2 begins with its dissociation into hydrogen cations (H^+) and perhydroxyl anion (HO_2^-), with the generation of H^+ ions reflecting its nature as a weak acid. The perhydroxyl anion subsequently reacts with another H_2O_2 molecule, leading to the formation of hydroxyl radicals (HO•) and perhydroxyl radicals (HO_2•). This chain reaction continues, generating additional perhydroxyl radicals and water. Ultimately, all H_2O_2 molecules decompose into water upon completion of the reaction [34]. In addition to pH, temperature significantly influences the decomposition rate of H_2O_2. Yazici and Deveci [35] reported that the decomposition rate increased by approximately 20-fold when the temperature was raised from 20 to 50 °C over a 3-hour period.

However, the bleaching (delignification) efficiency increases as the pH increases. This direct relationship between pH and bleaching efficacy has been well-documented in industrial bleaching processes involving cotton fibers and wood pulp [36]. In such applications, the pH of H_2O_2 solutions is intentionally raised, as the bleaching effectiveness of H_2O_2 is significantly enhanced at pH values above 10. At pH levels between 10 and 12, H_2O_2 begins to dissociate, and the perhydroxyl anion (HO_2^-) becomes the predominant species above pH 11. This anion is believed to play a key role in enhancing the bleaching power of the solution [37].

In **Figures 1** and **2**, the solid recovery rate increased, while delignification efficiency decreased when the H_2O_2 concentration was elevated to 10 % under treatment at 35 °C. This phenomenon may be attributed to the effect of pH on H_2O_2 decomposition and delignification efficiency, as discussed earlier. At the same temperature, higher H_2O_2 concentrations theoretically result in lower pH values. Although pH was not directly measured in this study, it is generally

accepted that a 10 % H_2O_2 solution exhibits a lower pH than a 2.5 % solution. The initial decomposition product, hydrogen cations (H^+), can impair the effectiveness of the alkali in the saponification reaction by neutralizing hydroxide ions (OH^-) derived from NaOH. This neutralization reduces the availability of OH^- ions, thereby decreasing lignin removal efficiency. Additionally, the bleaching effectiveness of H_2O_2 is reduced under more acidic conditions. As a result, a higher solid recovery rate was observed because a larger proportion of lignin remained intact within the solid residue. In contrast, elevated temperatures promote the efficiency of alkali pretreatment by enhancing the solvation and saponification of intermolecular ester bonds linking lignin, hemicellulose, and cellulose [30]. Furthermore, higher temperatures facilitate biomass swelling, which increases the accessibility of pretreatment chemicals to the internal structure of the biomass, ultimately resulting in more effective lignin removal.

Regarding cellulose content in the extracted solids, a longer residence time was required to achieve higher cellulose content at the lower treatment temperature (35 °C), regardless of the H_2O_2 concentration. However, at a higher temperature (60 °C), prolonged residence time resulted in cellulose loss across all H_2O_2 concentrations, as evidenced by lower cellulose content compared to samples treated at 50 °C. Notably, the highest lignin removal was also observed at 60 °C for all H_2O_2 concentrations, suggesting that both cellulose and lignin were significantly degraded at this elevated temperature and extended treatment duration. This finding aligns with observations by Suriyatem *et al.* [33], who reported that using high concentrations of H_2O_2 (up to 40 %, v/v) at 80 °C for 2 h led to a reduction in cellulose yield. The loss of cellulose was likely due to depolymerization of the cellulose macromolecules into shorter chains, which subsequently became solubilized in the liquid phase.

Interestingly, the present study found that the optimal condition for cellulose isolation—using 7.5 % H_2O_2 at 50 °C for 5 h—yielded the highest cellulose content (64 % by weight of the pretreated solid as shown in **Figure 4**). At 50 °C, the cellulose content was higher compared to treatments conducted at both 35 and 60 °C. This temperature-dependent variation in cellulose content can be attributed to the balance between delignification efficiency and cellulose degradation. At the lower temperature (35 °C), delignification was less effective, resulting in a higher retention of lignin (and likely hemicellulose) in the solid residue. Consequently, the overall proportion of cellulose in the pretreated solid was lower—below 30 wt%—as a significant portion of the solid mass consisted of non-cellulosic components. In contrast, at the higher temperature (60 °C), although delignification was more effective, cellulose depolymerization also occurred, leading to its solubilization into the liquid phase and a consequent reduction in cellulose yield. These findings suggest that overly severe conditions such as high H_2O_2 concentration, elevated temperature, and extended residence time can lead to cellulose loss in the pretreated durian rind. Therefore, the condition of 7.5 % H_2O_2 at 50 °C for 5 h was selected as optimal for cellulose extraction and used in subsequent experiments.

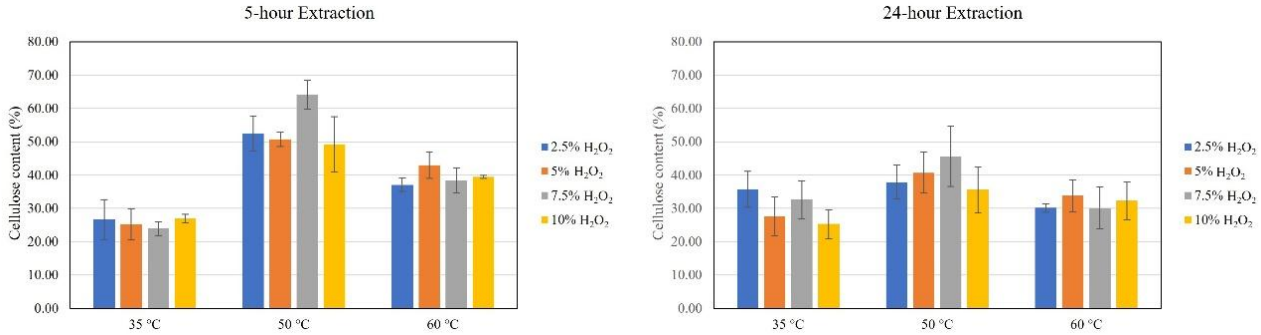

Figure 4 Cellulose content (wt%) in durian rind samples after extraction with 5 % NaOH in different concentrations of H_2O_2 at elevated temperatures for 5 and 24 h.

Fourier-transform infrared (FTIR) analysis of cellulose

Cellulose was isolated from durian rind samples under the optimal condition (5 % NaOH in 7.5 % H_2O_2, 50 °C, 5 h). The extracted cellulose was subsequently oven-dried, ground, and sieved to obtain 3 different particle size ranges: < 250 μm, 250 - 425 μm, and > 425 μm. Fourier-transform infrared (FTIR) spectroscopy and additional analyses to characterize their properties.

The FTIR spectra of the raw material (durian rind) and the extracted cellulose with varying particle sizes are shown in **Figure 5**. Absorption bands in the range of 3600 - 2800 cm^{-1} were observed in all samples, corresponding to the stretching vibrations of C-H and O-H groups [38]. Notably, several absorption bands present in the raw material were absent or altered in the spectra of the extracted cellulose, indicating chemical modifications to the polymer structure following alkali and hydrogen peroxide treatment. The FTIR spectra of the cellulose samples appeared similar across all particle sizes, suggesting that particle size had minimal influence on the overall chemical structure of the isolated cellulose.

In the raw material, distinct peaks at 1369 and 1026 cm^{-1} were observed, indicating a high content of uronic acids and pectin [39]. Hasem *et al*. [29] reported that durian rind from the D118 cultivar contained up to 73.67 % pectin by weight. These characteristic peaks were absent in the FTIR spectra of all cellulose samples following the extraction process used in this study, confirming the effective removal of pectin and related non-cellulosic components during pretreatment.

Regarding lignin, the peak at 1604 cm^{-1} representing aromatic skeletal vibrations was prominent in the raw material but significantly reduced in the spectra of the extracted cellulose. The absorption band at 1241 cm^{-1} in the native durian rind spectrum corresponds to aromatic skeletal vibrations and C-O stretching of the acetyl group in lignin [40,41]. This peak was absent from all cellulose sample spectra, indicating a substantial reduction in lignin content. The disappearance of these peaks suggests that lignin was effectively solubilized in the alkali and hydrogen peroxide solution, likely due to the cleavage of ether and ester linkages within the lignin structure by reactions with NaOH and H_2O_2. Only the peak at 1507 cm^{-1}, associated with C=C stretching in the aromatic rings of lignin, remained visible in the spectra of all cellulose samples [42]. This observation confirms a significant reduction in lignin content after alkali and hydrogen peroxide pretreatment, although complete lignin removal was not achieved under the given conditions. These qualitative FTIR results are consistent with the quantitative data presented in **Figure 2**, further confirming that a substantial portion of lignin was removed from the durian rind during the treatment process.

For hemicellulose, the carbonyl (C=O) stretching vibrations of carboxyl and acetyl groups appear as a peak at 1735 cm^{-1} [40]. This absorption band was absent in the spectra of all cellulose samples, indicating that these functional groups were effectively removed and solubilized into the liquid phase during pretreatment [41]. In the raw material spectrum, a small shoulder peak at 1043 cm^{-1} was observed, which is associated with xylan, a major component of hemicellulose [43,44]. A similar small shoulder peak at 1038 cm^{-1} was present in the spectra of all cellulose samples, suggesting the possible presence of minor carbohydrate impurities, such as residual hemicellulose, in the extracted cellulose.

The intensity of peaks corresponding to cellulose was markedly higher in all cellulose samples compared to the raw material prior to extraction. Specifically, the C-O-C stretching vibrations of β-(1,4)-glycosidic bonds in cellulose was identified by peaks at 1157, 1091, and 895 cm^{-1} [38,45]. In addition, a peak at 1316 cm^{-1} observed in all cellulose samples corresponds to CH_2 wagging vibrations in cellulose [46]. The intensity of FTIR absorption peaks is directly related to the amount of infrared radiation absorbed by the sample, which in turn reflects the abundance of the corresponding molecular functional groups. Therefore, an increase in peak intensity generally suggests a higher concentration of the associated functional groups.

However, no attempt was made in this study to quantitatively compare the concentration of functional groups before and after the extraction process. Moreover, aside from lignin removal (**Figure 2**) and cellulose content (**Figure 4**), no additional quantitative analyses were conducted to confirm the purity level of the extracted cellulose. As such, the exact purity of the cellulose could not be determined. Nevertheless, based on the FTIR results and gravimetric data, it can be

assumed that cellulose was significantly enriched in the samples following alkali and hydrogen peroxide treatment, relative to the raw material.

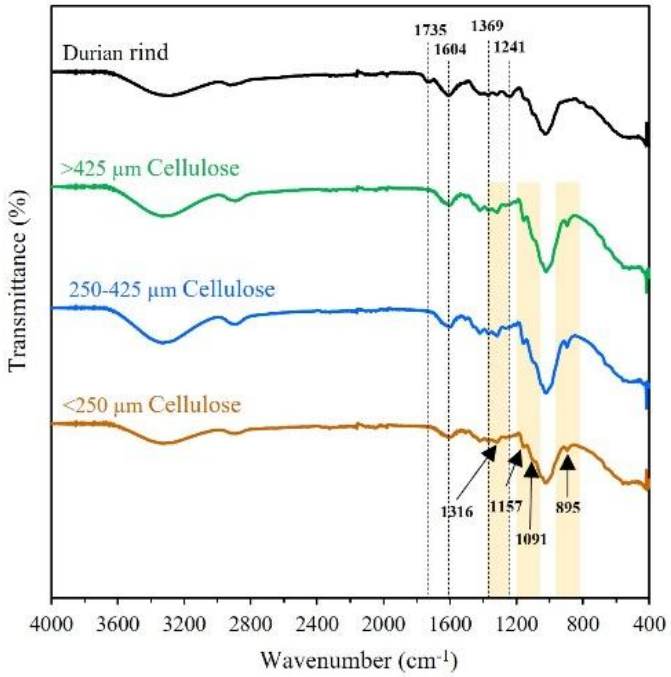

Figure 5 FTIR Spectra of durian rind (raw material) and cellulose with particle sizes <250 µm, 250 - 425 µm, and >425 µm.

X-ray diffraction (XRD) analysis of cellulose

Cellulose samples with different particle sizes were analyzed using X-ray diffraction (XRD) to determine their crystallographic structure and physical properties. Two distinct peaks were observed in the XRD patterns of all cellulose samples (**Figure 6**), which are characteristic of cellulose crystalline regions [24]. The crystallinity indices, calculated from the XRD peak areas, are presented in **Table 4**. These values ranged from 31.2 to 35.5 %. However, no clear correlation was observed between crystallinity and particle size. The influence of cellulose crystallinity on the performance of PLA/cellulose composites is further discussed in a later section of this study.

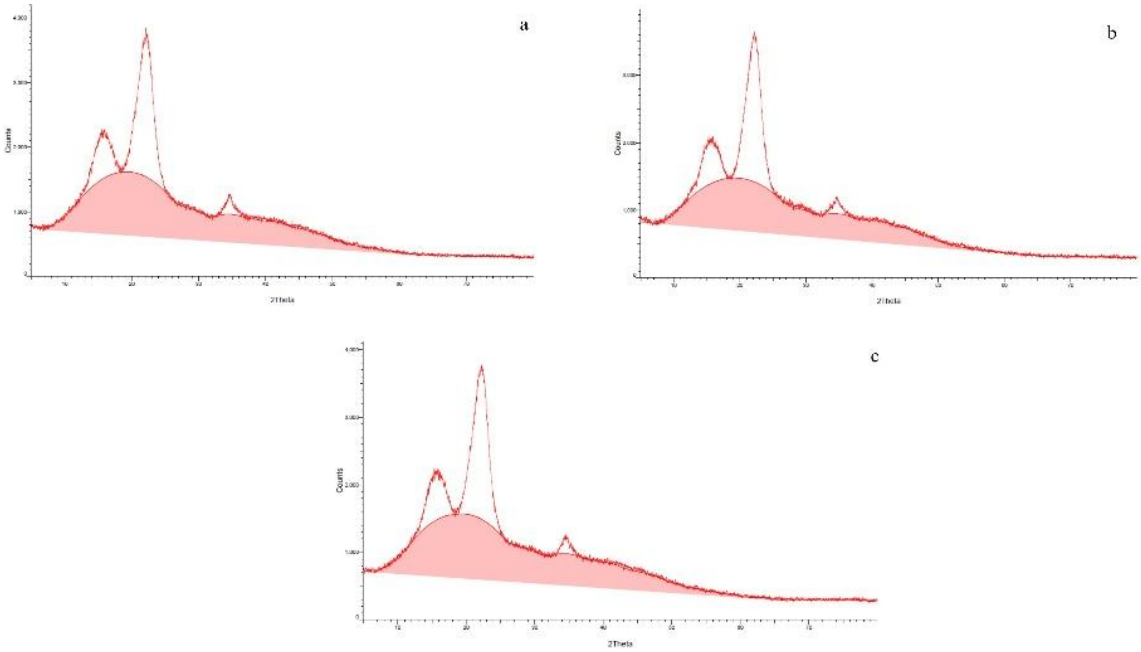

Figure 6 XRD chromatograms of cellulose with particle sizes (a) < 250 µm, (b) 250 - 425 µm, and (c) > 425 µm.

Table 4 Crystallinity of cellulose with different particle sizes. Data represent average ± 1 standard deviation.

Particle size of cellulose (µm)	Crystallinity (%)*
< 250	31.5 ± 0.8[a]
250 - 425	35.5 ± 0.4[b]
> 425	31.2 ± 0.6[a]

*Lowercase letter indicates significant difference ($p < 0.05$).

Morphological structure of cellulose

The morphological structures of cellulose samples with different particle sizes were examined using scanning electron microscopy (SEM), as shown in **Figure 7**. Following alkali and hydrogen peroxide pretreatment, as well as subsequent grinding and sieving, the cellulose samples exhibited rough surfaces and porous structures. These features are attributed to the combined effects of chemical and physical treatments. Similar surface morphologies have been reported in cellulose extracted from rice straw (10 cultivars) treated with alkali and hydrogen peroxide [22]. However, the cellulose sample with the largest particle size (> 425 µm) exhibited a more compact structure composed of fiber bundles, with no visible porous surface. This suggests that larger particles may retain more of their native structural integrity and are less affected by pretreatment and mechanical processing.

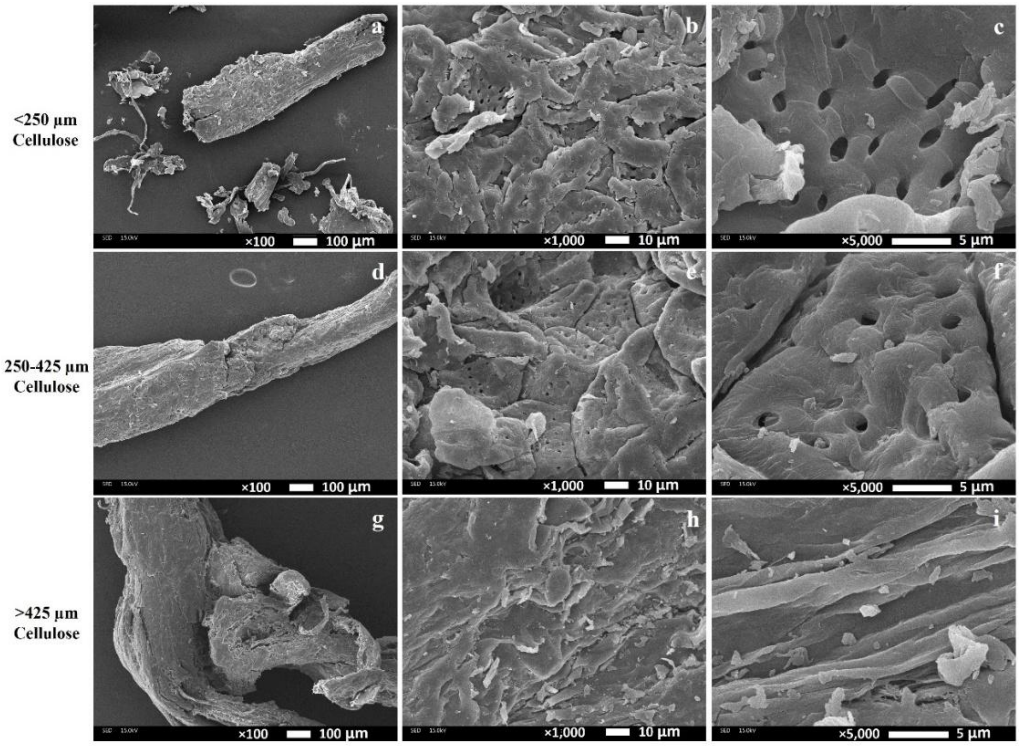

Figure 7 SEM micrographs of cellulose with particle sizes (a) - (c) < 250 µm, (d) - (f) 250 - 425 µm, and (g) - (i) > 425 µm at ×100, ×1000, and ×5000 magnifications.

Properties of PLA/cellulose composite

Visual appearance and color fading

As shown in **Figure 8**, the color appearance of the PLA/cellulose composites shifted from transparent/white to a darker shade with increasing cellulose content, indicating that cellulose acted as a pigment within the PLA matrix. However, there was no significant difference in the L* values among the different cellulose particle sizes.

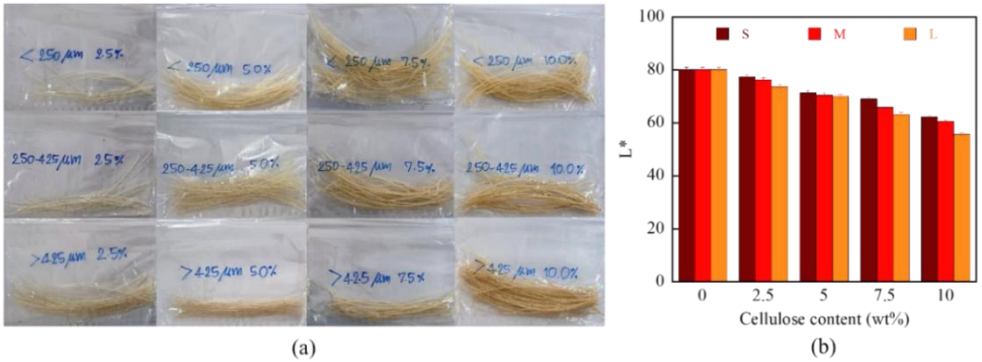

Figure 8 PLA/cellulose composites with different cellulose particle sizes and loading levels (a) visual appearance and (b) L* values.

Tensile properties

The mechanical properties of the PLA/cellulose composites, as influenced by cellulose particle size and loading, are summarized in **Table 5**. In general, all composite formulations exhibited higher Young's modulus (E) compared to neat PLA. The addition of 2.5 wt% cellulose led to a modest increase in E value by 3.23, 2.42, and 1.21 % for small (S), medium (M), and

large (L) cellulose particles, respectively. Increasing the cellulose content beyond 2.5 wt% resulted in only slight additional gains in modulus, with the maximum improvement observed at 7.5 wt%, showing an overall increase of 6.05 % across all particle sizes. These findings indicate that the composites became stiffer and more rigid than neat PLA [47,48].

Table 5 also shows that the tensile strength of PLA slightly decreased with the incorporation of 2.5 wt% cellulose across all particle sizes. As the cellulose content increased, tensile strength decreased more noticeably, by approximately 8 - 24 %, depending on particle size and loading level. The lowest tensile strength was recorded at 10 wt% loading with large (L) cellulose particles. Nevertheless, this value remained higher than that of commonly used polymers such as high-density polyethylene and PP [49,50].

Table 5 Tensile properties of PLA/cellulose composites with varying cellulose particle sizes and loadings. Data represent average ± 1 standard deviation.

Cellulose content (wt%)	Particle size	Tensile property*		
		Tensile modulus (GPa)	Tensile strength (MPa)	Elongation at break (%)
Neat PLA	-	2.48 ± 0.14^{a}	60.84 ± 2.33^{a}	4.61 ± 0.15^{a}
2.5	S	2.56 ± 0.19^{aA}	57.17 ± 3.56^{abA}	4.14 ± 0.16^{abA}
	M	2.54 ± 0.10^{aA}	56.83 ± 4.98^{abA}	3.97 ± 0.19^{abA}
	L	2.51 ± 0.07^{aA}	57.31 ± 3.02^{abA}	3.26 ± 0.20^{abA}
5.0	S	2.59 ± 0.11^{aA}	55.76 ± 2.16^{bA}	3.57 ± 0.57^{bcA}
	M	2.58 ± 0.12^{aA}	54.52 ± 3.11^{cAA}	3.24 ± 0.46^{bcA}
	L	2.56 ± 0.15^{aA}	50.66 ± 2.05^{bcB}	2.23 ± 0.36^{bcB}
7.5	S	2.63 ± 0.07^{a}	52.81 ± 1.68^{cA}	2.94 ± 0.11^{cdA}
	M	2.62 ± 0.20^{aA}	49.26 ± 2.04^{dB}	2.43 ± 0.40^{cdA}
	L	2.59 ± 0.18^{aA}	50.64 ± 1.51^{bcAB}	1.53 ± 0.28^{cdB}
10	S	2.49 ± 0.12^{aA}	47.05 ± 2.59^{dA}	2.20 ± 0.16^{dA}
	M	2.61 ± 0.08^{aA}	46.61 ± 3.14^{eA}	2.45 ± 0.44^{dA}
	L	2.60 ± 0.14^{aA}	46.32 ± 3.58^{cA}	1.02 ± 0.18^{dB}

*Lowercase letters indicate significant differences between cellulose contents compared with neat PLA. Uppercase letters indicate significant differences between cellulose particle sizes ($p < 0.05$).

A similar trend was observed in tensile elongation at break. These reductions in tensile strength and elongation are primarily attributed to poor interfacial adhesion between the hydrophobic PLA matrix and the hydrophilic cellulose filler, which limits efficient stress transfer and promotes interfacial debonding under mechanical loading [47,48]. This effect was more pronounced with larger cellulose particles, likely due to their lower specific surface area and less uniform dispersion in the PLA matrix. In contrast, smaller cellulose particles showed slightly better interfacial interaction, likely due to their higher surface area and greater potential for bonding with the polymer matrix [51].

Field-emission scanning electron microscopy (FE-SEM), as illustrated in **Figure 9(a)**, revealed the characteristic brittle fracture surface of neat PLA, displaying a smooth morphology indicative of rapid crack propagation and low energy absorption during failure. This observation is consistent with previous studies that attribute PLA's intrinsic brittleness to its high glass transition temperature and limited chain mobility [51]. Upon incorporation of cellulose particles (**Figures 9(b) - 9(d)**), the fracture surfaces exhibited distinct interfacial voids, suggesting poor interfacial adhesion between the PLA matrix and the hydrophilic cellulose filler. Similar findings were reported by Suryanegara *et al.* [52], who noted weak interfacial

bonding in PLA/cellulose composites due to the inherent incompatibility between the polymer and filler phases.

The observed void formation may also result from phase separation under mechanical stress during sample preparation. Due to the differences in mechanical behavior between PLA and cellulose, the applied load induces deformation at varying rates, leading to separation at the interface and highlighting the lack of compatibility. This phenomenon has been frequently documented in literature, where mismatches in polarity and stiffness between PLA and cellulose result in localized stress concentrations and act as initiation points for failure [47]. These findings underscore the need for effective compatibilization strategies, such as surface grafting or the use of coupling agents, to improve interfacial adhesion and promote uniform stress transfer within the composite matrix.

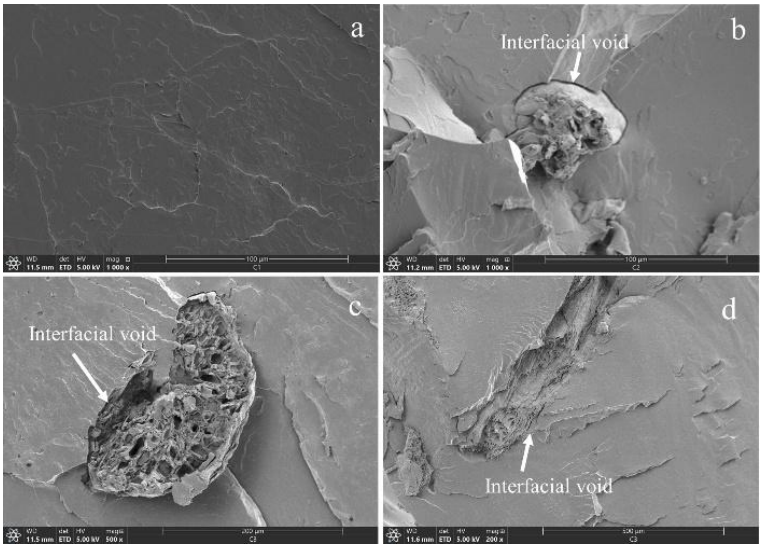

Figure 9 FE-SEM micrographs of (a) neat PLA, (b) PLA/< 250 μm (S) cellulose, (c) PLA/250 - 425 μm (M) cellulose, and (d) PLA/> 425 μm (L) cellulose composite.

Various approaches have been explored to enhance interfacial adhesion and improve the mechanical properties of PLA/cellulose composites. One notable method involves the use of polyamide amine (PAMAM) dendrimers as compatibilizers. Studies have shown that incorporating PAMAM into PLA/cellulose acetate (CA) blends significantly improves compatibility, leading to better dispersion of CA within the PLA matrix. This modification has been reported to result in a 551 % increase in toughness and a 141 % enhancement in tear strength. Moreover, the presence of PAMAM increases the hydrophobicity and oxygen permeability of the blend films, making them more suitable for applications such as food packaging [53].

Another approach involves surface modification of cellulose fibers through silanization. In one study, cotton fibers were subjected to sequential acid hydrolysis and silanization before being incorporated into PLA matrices. The silanization treatment enhanced the dispersion of the cellulose fibers and strengthened interfacial adhesion, resulting in increases in both Young's modulus and tensile strength at break compared to neat PLA [54]. Additionally, grafting polylactic acid onto microcrystalline cellulose (MCC) via melt copolycondensation has been investigated. The resulting MCC-g-PLA copolymers, when incorporated into PLA matrices, exhibited improved dispersion and interfacial compatibility. This modification also enhanced the melt strength and crystallization behavior of PLA, addressing some of its inherent limitations in processing and mechanical performance [55].

The incorporation of cellulose resulted in noticeable changes in the thermal behavior of PLA, as summarized in **Table 6**. Specifically, the glass transition temperature (T_g) of PLA increased slightly, by approximately 1 - 2 °C, with the addition of cellulose. Furthermore, the PLA composites exhibited earlier crystallization, occurring about 1 - 2 °C prior to that of neat PLA. A significant enhancement in the degree of

crystallinity (X_c) was also observed, with the highest increase found at 7.5 wt% cellulose loading using particle sizes smaller than 250 µm. These smaller cellulose particles were particularly effective in promoting crystallization. This enhancement in crystallinity can be attributed, in part, to findings from the FE-SEM analysis. As shown in **Table 6**, poor interfacial adhesion between the PLA and cellulose resulted in the formation of thermally insulated zones that impeded heat transfer from the PLA matrix to the cellulose. Consequently, the cellulose particles remained relatively cooler during heating and acted as efficient nucleation sites for PLA crystallization [56,57]. This nucleating effect is the primary contributor to the observed increase in X_c and may help reduce the injection molding cycle time [27].

Table 6 Thermal transition temperatures of neat PLA and PLA/cellulose composites.

Cellulose content (wt%)	Particle size (µm)	T_g (°C)	T_c (°C)	T_m (°C)	X_c (%)
0	-	60.1	114	153	3.96
	S	59.2	110	156	6.36
2.5	M	60.6	112	157	5.73
	L	60.4	111	156	5.52
	S	61.4	109	155	14.6
5.0	M	62.1	113	156	12.1
	L	61.9	113	157	11.5
	S	61.0	110	155	17.3
7.5	M	61.4	113	157	16.8
	L	61.9	112	155	14.7
	S	61.5	111	156	15.9
10	M	60.9	112	156	13.6
	L	61.3	113	157	11.9

Cellulose nanofibers (CNFs) have been incorporated into PLA matrices to evaluate their influence on crystallization behavior and mechanical properties. The addition of 3 wt% CNFs led to a 95 % increase in crystallinity compared to neat PLA, reaching a crystallinity of 44.2 %. This improvement was attributed to the strong nucleating effect of CNFs, which accelerated the crystallization rate of PLA by a factor of 65. Mechanical testing further demonstrated enhanced tensile strength and modulus in the CNF-reinforced PLA, indicating that CNFs function effectively as both nucleating agents and reinforcing fillers [58]. Similarly, Chu *et al*. [59] investigated the incorporation of nanofibrillated cellulose (NFC) into PLA matrices. Their study showed that adding 10 wt% NFC significantly increased the crystallization temperature and overall crystallinity of the PLA composite. This improvement was attributed to the heterogeneous nucleation provided by NFC, which promoted more efficient crystallization. These findings collectively underscore the potential of cellulose-based nanomaterials as effective nucleating agents for improving both the crystallization behavior and mechanical performance of PLA composites. However, the loading level of these nanomaterials is critical, as excessive amounts may lead to agglomeration, diminishing their reinforcing and nucleating effects. Further research into surface modification techniques and dispersion strategies could enhance compatibility and maximize the functional benefits of cellulose-reinforced PLA composites. Additionally, applying post-processing strategies such as annealing or increasing the molding time may offer further improvements in crystallinity and material performance.

Conclusions

Durian rind demonstrates strong potential as a sustainable source of cellulose within the framework of

a circular economy. Through an efficient single-step alkali and hydrogen peroxide pretreatment, approximately 50 % of the dry weight of durian rind was recovered as extracted cellulose. This translates to an estimated yield of 500 kg of cellulose from 1 ton of durian rind waste. The extracted cellulose was successfully employed as a reinforcing agent in PLA-based composites. The particle size and loading content of the cellulose were found to significantly influence the composite properties. Young's modulus increased with cellulose incorporation, regardless of particle size or loading level, indicating improved stiffness compared to neat PLA. However, the inherent incompatibility between hydrophilic cellulose and hydrophobic PLA resulted in interfacial voids, which contributed to reductions in tensile strength and elongation at break. Despite these reductions, the mechanical performance remained superior to that of conventional polymers such as HDPE and PP. Therefore, Additionally, the degree of crystallinity in PLA/cellulose composites was greater than that of neat PLA, particularly when smaller cellulose particles were used. This enhancement may support improved thermal stability and processing behavior. The composites appear suitable for single-use applications such as agricultural trays, biodegradable cutlery, and straws. The use of larger cellulose particle sizes offers practical benefits, including reduced energy consumption for grinding and simplified sample preparation. Moreover, the presence of interfacial voids may theoretically accelerate biodegradation, offering additional environmental advantages. Future work should focus on improving interfacial compatibility between PLA and cellulose. Strategies such as the addition of compatibilizers, use of coupling agents, or chemical surface modification may enhance mechanical performance and expand the potential of these composites for more demanding applications, including durable food packaging.

Acknowledgements

This research was financially supported by the Faculty of Agricultural Product Innovation and Technology, Srinakharinwirot University, Thailand [Grant No. 401/2563].

Declaration of Generative AI in Scientific Writing

In this paper, the AI tool was used to support the grammatical correction. The authors confirm that all intellectual content, interpretations, data analysis, and conclusions were conceived and verified by the authors themselves. No AI tools were used to generate data, create images, perform experimental procedures, or interpret results. The authors take full responsibility for the integrity, originality, and accuracy of the content presented in this paper.

CRediT author statement

Nawadon Petchwattana: Writing – review & editing, Visualization, Methodology, Investigation, Software, Data curation.

Kamonchai Cha-aim: Resources, Investigation, Formal analysis, Data curation.

Khanet Rodphool and Jakkid Sanetuntikul: Resources, Visualization, Investigation, Formal analysis.

Puttaraksa Sang-on and Tuangphon Lapsarn: Data curation, Visualization.

Supaporn Sophonputtanaphoca: Writing – review & editing, Validation, Supervision, Resources, Project administration, Methodology, Funding acquisition, Conceptualization.

References

[1] G Cazacu and V Popa. *Blends and composites based on cellulose material. In*: S Dumitriu (Ed.). Polysaccharides structural diversity and functional versatility. 2nd eds. CRC Press, Boca Raton, 2004.

[2] P Rai, S Mehrotra, S Priya, E Gnansounou and SK Sharma. Recent advances in the sustainable design and applications of biodegradable polymers. *Bioresource Technology* 2021; **325**, 124739.

[3] CG Silva, PAL Campini, DB Rocha and DS Rosa. The influence of treated eucalyptus microfibers on the properties of PLA biocomposites. *Composites Science and Technology* 2019; **179**, 54-62.

[4] H Ebadi-Dehaghani, HA Khonakdar, M Brarikani and SH Jafari. Experimental and theoretical analyses of mechanical properties of PP/PLA/clay nanocomposites. *Composites: Part B: Engineering* 2015; **69**, 133-144.

[5] JC Posada, LY Jaramillo, EM Cadena and LA Garcia. Bio-based composites from agricultural wastes: Polylactic acid and bamboo *Guadua angustifolia*. *Journal of Composite Materials* 2015; **50(23)**, 3229-3237.

[6] HPSA Khalil, AH Bhat and AFI Yusra. Green composites from sustainable cellulose nanofibrils: A review. *Carbohydrate Polymers* 2012; **87(2)**, 963-979.

[7] M Luddee, S Pivsa-Art, S Sirisansaneeyakul and C Pechyen. Particle size of ground bacterial cellulose affecting mechanical, thermal, and moisture barrier properties of PLA/BC biocomposites. *Energy Procedia* 2014; **56**, 211-218.

[8] AP Mathew, K Oksman and M Sain. The effect of morphology and chemical characteristics of cellulose reinforcements on the crystallinity of polylactic acid. *Journal of Applied Polymer Science* 2006; **101(1)**, 300-310.

[9] K Halász and L Csóka. Plasticized biodegradable poly(lactic acid) based composites containing cellulose in micro- and nanosize. *Journal of Engineering* 2013; **2013**, 329379.

[10] U Saeed. Wood cellulose fibers reinforced polylactic acid composite: Mechanical, thermomechanical characteristics and orientation of fiber. *AIMS Materials Science* 2020; **7(1)**, 9-23.

[11] ISMA Tawakkal, RA Talib, K Abdan and CN Ling. Mechanical and physical properties of kenaf-derived cellulose (KDC)-filled polylactic acid (PLA) composites. *BioResources* 2012; **7(2)**, 1643-1655.

[12] MM Ali, N Hashim, SA Aziz and O Lasekan. Exploring the chemical composition, emerging applications, potential uses, and health benefits of durian: A review. *Food Control* 2020; **113**, 107189.

[13] MR Manshor, H Anuar, MNN Aimi, MIA Fitrie, WBW Nazri, SM Sapuan, YA El-Shekeil and MU Wahit. Mechanical, thermal and morphological properties of durian skin fibre reinforced PLA biocomposites. *Materials and Design* 2014; **59**, 279-286.

[14] R Jumaidin, LW Whang, RA Ilyas, KZ Hazrati, KZ Hafila, T Jamal and RA Alia. Effect of durian peel fiber on thermal, mechanical, and biodegradation characteristics of thermoplastic cassava starch composites. *International Journal of Biological Macromolecules* 2023; **250**, 126295.

[15] MC Lee, SC Koay, MY Chan, HL Choo, MM Pang, PM Chou and KY Tshai. Properties of poly(lactic acid)/durian husk fiber biocomposites: Effects of fiber content and processing aid. *Journal of Thermoplastic Composite Materials* 2020; **33(11)**, 1518-1532.

[16] S Charoenvai. *New insulating materials: Binderless particleboard from durian peel. In*: SY Chang, SKA Bahar and J Zhao (Eds.). Advances in civil engineering and building materials. Taylor and Francis Group, London, 2013, p. 119-123.

[17] P Penjumras, RA Rahman, RA Talib and K Abdan. Mechanical properties and water absorption behaviour of durian rind cellulose reinforced poly(lactic acid) biocomposites. *International Journal on Advanced Science, Engineering and Information Technology* 2015; **5(5)**, 343-349.

[18] A Sluiter, B Hames, D Hyman, C Payne, R Ruiz, C Scarlata, J Sluiter, D Templeton and J Wolfe. *Determination of total solids in biomass and total dissolved solids in liquid process samples: Laboratory Analytical Procedure (LAP), Technical Report NREL/TP-510-42621*. National Renewable Energy Laboratory, Golden, Colorado, 2008.

[19] A Sluiter, B Hames, R Ruiz, C Scarlata, J Sluiter and D Templeton. *Determination of ash in biomass: Laboratory Analytical Procedure (LAP), Technical Report NREL/TP-510-42622*. National Renewable Energy Laboratory, Golden, Colorado, 2008.

[20] A Sluiter, R Ruiz, C Scarlata, J Sluiter and D Templeton. *Determination of extractives in biomass: Laboratory Analytical Procedure (LAP), Technical Report NREL/TP-510-42619*. National Renewable Energy Laboratory, Golden, Colorado, 2008.

[21] A Sluiter, B Hames, R Ruiz, C Scarlata, J Sluiter, D Templeton and D Crocker. *Determination of structural carbohydrates and lignin in biomass: Laboratory Analytical Procedure (LAP), Technical Report NREL/TP-510-42618*. National

Renewable Energy Laboratory, Golden, Colorado, 2012.

[22] S Sophonputtanaphoca, P Chutong, K Cha-aim and P Nooeaid. Potential of Thai rice straw as a raw material for the synthesis of carboxymethylcellulose. *International Food Research Journal* 2019; **26(3)**, 969-978.

[23] P Rachtanapun, S Luangkamin, K Tanprasert and R Suriyatem. Carboxymethyl cellulose film from durian rind. *LWT - Food Science and Technology* 2012; **48(1)**, 52-58.

[24] N Haleem, M Arshad, M Shahid and MA Tahir. Synthesis of carboxymethyl cellulose from waste of cotton ginning industry. *Carbohydrate Polymers* 2014; **113**, 249-255.

[25] N Petchwattana, P Naknaen and B Narupai. Combination effects of reinforcing filler and impact modifier on the crystallization and toughening performances of poly(lactic acid). *Express Polymer Letters* 2020; **14(9)**, 848-859.

[26] S Jia, Y Chen, J Bian, H Pan, X Wang, L Zhao, L Han, H Zhang, L Dong and H Zhang. Preparation and properties of poly(L-lactic acid) blends with excellent low-temperature toughness by blending acrylic ester-based impact resistance agent. *International Journal of Biological Macromolecules* 2021; **183**, 1871-1880.

[27] N Petchwattana and B Narupai. Synergistic effect of talc and titanium dioxide on poly(lactic acid) crystallization: An investigation on the injection molding cycle time reduction. *Journal of Polymers and the Environment* 2019; **27**, 837-846.

[28] SR Masrol, MHI Ibrahim and S Adnan. Chemi-mechanical pulping of durian rinds. *Procedia Manufacturing* 2015; **2**, 171-180.

[29] NH Hasem, SFZM Fuzi, F Kormin, MFA Bakar and SF Sabran. Extraction and partial characterization of durian rind pectin. *IOP Conference Series: Earth and Environmental Science* 2019; **269**, 12019.

[30] S Sophonputtanphoca, K Srigatmaneerat and K Kruakrut. Effect of low temperatures and residence times of pretreatment on glucan reactivity of sodium hydroxide-pretreated rice straw. *Walailak Journal of Science and Technology* 2018; **15(4)**, 313-323.

[31] FM Giro, C Fonseca, F Carvalheiro, LC Duarte, S Marques and R Bogel-Lucasik. Hemicelluloses for fuel ethanol: A review. *Bioresource Technology* 2010; **101(13)**, 4775-4800.

[32] Y Su, R Du, H Guo, M Cao, Q Wu, R Su, W Qi and Z He. Fractional pretreatment of lignocellulose by alkaline hydrogen peroxide: Characterization of its major components. *Food and Bioproducts Processing* 2015; **94**, 322-330.

[33] R Suriyatem, N Noikang, T Kankam, K Jantanasakulwong, N Leksawasdi, Y Phimolsiripol, C Insomphun, P Seesuriyachan, T Chaiyaso, P Jantrawut, SR Sommano, TMP Ngo and P Rachtanapun. Physical properties of carboxymethyl cellulose from palm bunch and bagasse agricultural wastes: Effect of delignification with hydrogen peroxide. *Polymers* 2020; **12(7)**, 1505.

[34] CRG Torres, E Crastechini, FA Feitosa, CR Pucci and AB Borges. Influence of pH on the effectiveness of hydrogen peroxide whitening. *Operative Dentistry* 2014; **39(6)**, E261-E268.

[35] EY Yazici and H Deveci. Factors affecting decomposition of hydrogen peroxide. *In:* Proceedings of the 12th International Mineral Processing Symposium, Cappadocia-Nevşehir, Turkey. 2010, p. 609-616.

[36] R Hage, JWD Boer, F Gaulard and K Maaijen. Manganese and iron bleaching and oxidation catalysts. *Advances in Inorganic Chemistry* 2013; **65**, 85-116.

[37] E Trautmann, T Attin, D Mohn and M Zehnder. Hydrogen peroxide versus sodium hypochlorite: All a matter of pH? *Journal of Endodontics* 2021; **47(2)**, 297-302.

[38] Q Cai, Z Fan, J Chen, W Guo, F Ma, S Sun, L Hu and Q Zhou. Dissolving process of bamboo powder analyzed by FT-IR spectroscopy. *Journal of Molecular Structure* 2018; **1171**, 639-643.

[39] M Chylińska, M Szymańska and A Zdunek. FT-IR and FT-Raman characterization of non-cellulosic polysaccharides fractions isolated from plant cell wall. *Carbohydrate Polymers* 2016; **154**, 48-54.

[40] RR Rizkiansyah, Y Mardiyati, A Hariyato, S Steven and T Dirgantara. Non-wood paper from

coffee pulp waste: How its performance as coffee filter. *Cleaner Materials* 2024; **12**, 100241.

[41] BS Yew, M Muhamad, SB Mohamed and FH Wee. Effect of alkaline treatment on structural characterization, thermal degradation and water absorption ability of coir fibre polymer composites. *Sains Malaysiana* 2019; **43(3)**, 653-659.

[42] RG Candido and AR Gonçalves. Synthesis of cellulose acetate and carboxymethylcellulose from sugarcane straw. *Carbohydrate Polymers* 2016; **152**, 679-686.

[43] I Egüés, C Sanchez, I Mondragon and J Labidi. Effect of alkaline and autohydrolysis processes on the purity of obtained hemicelluloses from corn stalks. *Bioresource Technology* 2012; **103(1)**, 239-248.

[44] RC Sun and J Tomkinson. Characterization of hemicelluloses obtained by classical and ultrasonically assisted extractions from wheat straw. *Carbohydrate Polymers* 2002; **50(3)**, 263-271.

[45] M Li, LJ Wang, D Li, YL Cheng and B Adhikari. Preparation and characterization of cellulose nanofibers from de-pectinated sugar beet pulp. *Carbohydrate Polymers* 2014; **102**, 136-143.

[46] P Penjumras, RBA Rahman, RA Talib and K Abdan. Extraction and characterization of cellulose from durian rind. *Agriculture and Agricultural Science Procedia* 2014; **2**, 237-243.

[47] N Petchwattana, W Channuan, P Naknaen and B Narupai. 3D printing filaments prepared from modified poly (lactic acid)/teak wood flour composites: An investigation on the particle size effects and silane coupling agent compatibilisation. *Journal of Physical Science* 2019; **30(2)**, 169-188.

[48] VU Siddiqui, J Yusuf, SM Sapuan, MZ Hasan, MMM Bistari and ZG Mohammadsalih. Mechanical properties and flammability analysis of wood fiber filled polylactic acid (PLA) composites using additive manufacturing. *Journal of Natural Fibers* 2024; **21(1)**, 2409868.

[49] J Sanetuntikul, B Narupai and N Petchwattana. A circular economy use of post-consumer polypropylene packaging for low thermal conductive and fire-retardant building material applications. *Journal of Renewable Materials* 2023; **11(9)**, 3567-3582.

[50] N Petchwattana, S Covavisaruch and S Chanakul. Mechanical properties, thermal degradation and natural weathering of high-density polyethylene/ rice hull composites compatibilized with maleic anhydride grafted polyethylene. *Journal of Polymer Research* 2012; **19**, 9921.

[51] M Jamshidian, EA Tehrany, M Imran, M Jacquot and S Desobry. Poly-lactic acid: Production, applications, nanocomposites, and release studies. *Comprehensive Reviews in Food Science and Food Safety* 2010; **9(5)**, 552-571.

[52] L Suryanegara, AN Nakagaito and H Yano. The effect of crystallization of PLA on the thermal and mechanical properties of microfibrillated cellulose -reinforced PLA composites. *Composites Science and Technology* 2009; **69(7-8)**, 1187-1192.

[53] Y Huang, Y Jin, B Wang, H Tian, Y Weng and S Men. Compatibilization and toughening of biodegradable polylactic acid/cellulose acetate films by polyamide amine dendrimers. *Journal of Polymers and the Environment* 2022; **30**, 1758-1771.

[54] RS Araújo, LC Ferreira, CC Rezende, MFV Marques, ME Errico, R Avolio, M Avella, G Gentile and P Russo. Poly(lactic acid)/cellulose composites obtained from modified cotton fibers by successive acid hydrolysis. *Journal of Polymers and the Environment* 2018; **26**, 3149-3158.

[55] S Hua, F Chen, ZY Liu, W Yang and MB Yang. Preparation of cellulose-graft-polylactic acid via melt copolycondensation for use in polylactic acid based composites: Synthesis, characterization and properties. *RSC Advances* 2016; **6**, 1973-1983.

[56] EH Backes, LDN Pires, LC Costa, FR Passador and LA Pessan. Analysis of the degradation during melt processing of PLA/Biosilicate® composites. *Journal of Composites Science* 2019; **3(2)**, 52.

[57] N Petchwattana, B Sukkaneewat, P Naknaen, J Sanetuntikul and E Jansri. Synergistic effects of bio-plasticizer and core-shell rubber on poly(lactic acid) toughness for sustainable flexible packaging applications. *Journal of Applied Polymer Science* 2022; **139(14)**, 51894.

[58] SS Shazleen, TAT Yasim-Anuar, NA Ibrahim, MA Hassan and H Ariffin. Functionality of cellulose nanofiber as bio-based nucleating agent and nano-reinforcement material to enhance crystallization and mechanical properties of polylactic acid nanocomposite. *Polymers* 2021; **13(3)**, 389.

[59] H Chu, Z Chen, Y Chen, D Wei, Y Liu and H Zhao. Mechanical properties and crystallinity of specific PLA/cellulose composites by surface modification of nanofibrillated cellulose. *Polymers* 2024; **16(17)**, 2474.